---

**Article:**
Eraslan, S., Gitman, I.M., Askes, H. et al. (1 more author) (2022) Determination of representative volume element size for a magnetorheological elastomer. Computational Materials Science, 203. 111070. ISSN 0927-0256

https://doi.org/10.1016/j.commatsci.2021.111070

---

# Graphical Abstract

**Determination of Representative Volume Element Size for a Magnetorheological Elastomer**

Sinan Eraslan, Inna M. Gitman, Harm Askes, René de Borst

No graphical abstract

# Highlights

**Determination of Representative Volume Element Size for a Magnetorheological Elastomer**

Sinan Eraslan, Inna M. Gitman, Harm Askes, René de Borst

- A numerically-statistical analysis has been used to determine lower bounds of the RVE size for magnetorheological elastomers (MRE) material, resulting in different RVE sizes for different phenomena: purely elastic, purely magnetic, and coupling behaviour in the material. Difference between aforementioned RVE sizes has been analysed and it was suggested that using the largest determined RVE size can be used in gradient enriched governing equations to introduce the information from the underlying micro level.
- The formalistic approach showed that the contrast in material properties of the constituents can affect the minimum RVE sizes. It has been concluded that for more heterogeneity in material properties, larger sizes of the associated RVE are obtained.
- While there is a converging trend for purely elastic and purely magnetic RVEs, coupling RVEs show a non-convergent trend in the range of assumed larger contrast values. Given that the difference between convergent and non-convergent trends occurs for extremely large contrast, for practical purposes one may assume same RVE size for all.
- A piezomagnetic continuum model has been developed with gradients of strain, piezomagnetic coupling and magnetic field whereby the microstructural length scale parameters are expressed in terms of RVE sizes.

# Determination of Representative Volume Element Size for a Magnetorheological Elastomer

Sinan Eraslan[a,*], Inna M. Gitman[a], Harm Askes[b], René de Borst[b]

[a]*The University of Sheffield, Department of Mechanical Engineering, Sheffield, S1 3JD, , United Kingdom*
[b]*The University of Sheffield, Department of Civil and Structural Engineering, Sheffield, S1 3JD, , United Kingdom*

**Abstract**

Smart composite materials have been an active field of research in the last few decades. Magnetorheological elastomers (MREs) are examples of such smart composites and they show a coupling between magnetism and elasticity. MREs are heterogeneous materials and they consist of magnetic particles and a silicone-based elastomer. To describe and predict the behaviour of the macroscopic continuum accurately, microstructural information needs to be taken into account in the analysis of heterogeneous materials. Therefore, a combined approach called multi-scale analysis is used to consider various scales of observation simultaneously. The concept of Representative Volume Element (RVE) is typically employed by multi-scale approaches to describe the micro scale, and thus the size of RVE becomes a model parameter in such techniques. This has motivated the determination of the RVE size and the derivation of magnetoelastic constitutive relations in terms of the RVE sizes in our paper. The finite element method and a statistical analysis based on the coefficient of variation have been used to determine the RVE size of MREs. The results show that it is possible to determine a lower bound of the RVE size for an MRE. Furthermore, a parametric study has been conducted to examine the sensitivity of the RVE size on the different material properties of the constituents. It was found that the RVE size is primarily set by the *contrast* of the different material properties, i.e. the stiffness, permeability and magnetoelastic coupling coefficients.

*Keywords:* Magnetorheological elastomers, Representative Volume Element, Finite element, Second-order homogenisation, Length Scale, Gradient elasticity

## 1. Introduction

Stimuli-responsive composite materials have been of great interest to the engineering community in the last few decades due to their controllable/adjustable behaviours and properties. These materials can respond to external effects such as temperature, light, pH, electric or magnetic field [1, 2]. Magnetorheological elastomers (MREs) are one type of such smart composites. They are generally manufactured by dispersion of magnetic particles in a silicone-based elastomer. These materials show a coupling between magnetism and elasticity via the magnetostriction effect [1, 2, 3, 4]. Magnetostriction is the ability of ferromagnetic materials to realise a change in material shape when a magnetic field is applied, which is called the direct magnetostrictive effect. By subjecting a magnetic field to an MRE, the particles will show magnetostriction, and the polymer matrix may experience forces due to this phenomenon. As a result, the composite material will deform [4, 5]. This coupling phenomenon opens up a variety of potential applications in many engineering fields, including actuators, sensors, vibration isolation and control, sensing of ultrasonic waves, and dialysis membranes in biomedical field [1, 2, 4, 6, 7, 8]. Various magnetic materials such as Terfenol-D, cobalt ferrite, certain earth metals and iron alloys can be used as magnetic filler with several alternatives of an elastic matrix such as natural rubber, silicone rubber or polyurethane [1, 3, 9, 10].

*Corresponding author:
Sinan Eraslan
Email adress: seraslan1@sheffield.ac.uk

Depending on the distribution of the particles, on a macro level these materials can be categorised as anisotropic or isotropic. Various reviews exist on the fundamentals of MREs, their production, modelling and applications. Thévenot et al. [1] and Filipcsei et al. [2] have treated magnetic responsive polymer composites (MRPCs) by covering different types of MRPCs, fabrication methods, detailed examples about the preparation steps and used products. Elhajjar et al. [4] evaluated the literature on magnetostrictive polymer composites (MPCs) after 2000 and presented progress and the current state of those materials. Some examples of different compositions (such as cobalt ferrites, Terfenol-D alloys and carbonyl iron) and their properties have been given in this review. Lastly, an overview from Ekreem et al. [5] explained how magnetostriction occurs. The advantages and disadvantages of the measurement procedures were compared to conclude the most common and sensitive methods.

After the introduction in the late 1990s, researchers have developed macroscopic and microscopic material models of ferrogels and elastomers. Camp and Wood [9] presented a microscopic model to study the relationship between features of the microstructure and physical properties of the ferrogels by using Monte Carlo computer simulations. It was shown that the elastic modulus can be controlled by applying a uniform magnetic field to the samples at the gel-formation stage. A macroscopic model has been proposed by Attaran et al. [11] to capture the mechanical deformation of ferrogels. The authors have simplified a previously developed continuum model for this reduced form, and it was reported that this reduced model shows good agreement with the experimental results. Another microscopically motivated approach has been proposed by Kalina et al. [12] to study the deformation behaviour of isotropic and anisotropic MREs. Raikher and Stolbov [13] have followed a continuum approach for MREs by considering them as a homogeneous elastic and isotropically magnetisable medium. Despite some limitations and drawbacks, the model is able to reproduce experimental results with acceptable accuracy.

The particle distribution plays a significant role in the magnetostriction of MREs as well as size, shape and volume fraction of the particles. On the micro scale a Representative Volume Element (RVE) approach is typically used to model materials. Here, an RVE is the smallest specimen of a material, which is large enough to be constitutively valid [14]. Metsch et al. [15] have modelled a range of RVEs based on a microscopically motivated continuum approach to investigate microstructural interactions. By applying varying amplitudes of the magnetic field, deformation of the isotropic and anisotropic RVE samples has been analysed for different volume fractions of the magnetic particles. This model is capable of describing magnetostriction by showing good agreement with the experimental results in the literature. Sun et al. [16] have proposed another RVE approach to investigate the effective mechanical properties of anisotropic MREs under plane stress conditions. The influence of some parameters such as magnetic field intensity, particle diameter and distance between the particles were examined and resulted in a positive correlation between shear modulus and field intensity/particle diameter, and inverse proportionality to the distance between the particles.

In addition to numerical models, experimental studies have been carried out for MREs. Li and Zhang [17] have proposed an experimental and theoretical model, where an optimum volume fraction was calculated for magnetic particles that leads to an improvement in magnetorheological effects. Borin et al. [18] have investigated the mechanical stress that results from the magnetostriction of hybrid magneto-elastic materials. In the experimental setup, two different types of magnetic particles (CI powder and NdFeB) and a polymer host (PDSM silicone) were used. They concluded that a measurable strictional reaction can be observed only when the specimens are filled with hard magnetic particles. This means that magnetic susceptibility of the constituents has a significant role in striction behaviour. An innovative fabrication method has been given by Li et al. [10]. They have demonstrated that 3D printing can be used to create anisotropic MREs without the need to use an external magnetic field. This study presents a new type of MRE manufacturing method, and it has been observed that some printing parameters, such as feed rate, extrusion pressure, and initial height have a significant effect on the properties of the MREs. In the experiments, it has been shown that damping capacity and dynamic stiffness of the 3D printed MREs could be tuned by applying a moderate external magnetic field. The above overview shows the importance of microstructural properties on the overall behaviour of MREs and, thus, the importance of capturing these microstructural properties in mechanical models.

In the analysis of heterogeneous materials such as MREs, capturing microstructural information in the macroscopic continuum has a significant role in accurately describing and predicting the response of the materials. For this reason, various scales need to be studied simultaneously through a combined approach, known as multi-scale analysis [19]. Homogenisation is a multi-scale approach in which a heterogeneous material model is described at the lower scale (micro-level). In analytical homogenisation approaches, the unit cell (RVE) is considered as model input; thus, the RVE size becomes a model parameter. As it has already been shown in [20, 21, 14], there is a link between the RVE size on the micro-scale and additional length scale parameters employed in nonlocal continua on the

macro-scale. Nonlocal continuum theories have been proposed by several authors to include the information from the micro-scale to the macroscopic continuum via additional material constants such as length scale parameters or time scale parameters (for dynamic analysis) [8, 20, 21]. However, these studies dealt with a purely mechanical response, and the extension to coupled physics (such as magnetoelasticity) was not addressed.

This study seeks to determine the RVE size for an MRE, by analysing the influence of the constituents' properties on this model parameter. In section 2, a finite element implementation will be adopted to obtain a microscopic boundary value problem to be used in the statistical analysis for RVE size determination. In section 3, numerical results and discussions of two-dimensional magnetoelastic RVEs will be given by covering the RVE size dependence on the material properties of the constituents. In section 4, macro-level magnetoelastic constitutive relation with internal length scale parameters will be derived by considering the RVE approach and second-order homogenisation scheme. Finally, some closing remarks are presented in section 5.

## 2. Formulation and Introduction of Methodology

Magnetostrictive materials show non-linear material behaviour, but they are biased by applying a magnetic field and mechanical compressive stress in most applications. This bias allows to describe the material behaviour by using linear piezomagnetic equations. By assuming a static magnetic field (curl-free), the constitutive equations of a linear piezomagnetic medium in classical continuum theory can be written as [8, 22, 23, 24]

$$\begin{aligned} \sigma_{ij} &= C_{ijkl}\varepsilon_{kl} - Q_{nij}H_n \\ B_i &= Q_{ikl}\varepsilon_{kl} + \mu_{in}H_n \end{aligned} \tag{1}$$

where $\sigma$ and $B$ are the stress tensor and magnetic induction, $C$ and $Q$ are the stiffness tensor and piezomagnetic coupling tensor, $\mu$ is the magnetic permeability, and $\varepsilon$ and $H$ are strain and magnetic field respectively.

In a multi-scale approach, micro and macro scales link to each other by model parameters. This approach considers material on the microscopic level to reflect the real structure of heterogeneous material by considering each component's configuration and constitutive properties explicitly. Conversely, material is modelled as homogeneous with effective properties and model parameters on the macroscopic level. At this point, the concept of RVE is typically used to describe the micro scale. The RVE must be satisfactorily smaller than macroscopic dimensions, but it must have sufficient information about the microstructure [21, 14]. Thus, the size of RVE becomes a model parameter in the multi-scale approach. This approach brings the advantage of computational efficiency with an accurate description of the material behaviour on the macro-level.

In the multi-scale analysis, the macroscopic stress and induction can be defined as the volume average of the microscopic counterparts in the RVE and denoted as

$$\begin{aligned} \sigma_{ij}^{\mathrm{M}} &= \frac{1}{\mathrm{V_{RVE}}}\int_{\mathrm{V_{RVE}}} \sigma_{ij}^{\mathrm{m}}\,dV = \frac{1}{\mathrm{V_{RVE_1}}}\int_{\mathrm{V_{RVE_1}}} C_{ijkl}^{\mathrm{m}}\varepsilon_{kl}^{\mathrm{m}}\,dV - \frac{1}{\mathrm{V_{RVE_2}}}\int_{\mathrm{V_{RVE_2}}} Q_{nij}^{\mathrm{m}}H_n^{\mathrm{m}}\,dV \\ B_i^{\mathrm{M}} &= \frac{1}{\mathrm{V_{RVE}}}\int_{\mathrm{V_{RVE}}} B_i^{\mathrm{m}}\,dV = \frac{1}{\mathrm{V_{RVE_3}}}\int_{\mathrm{V_{RVE_3}}} Q_{ikl}^{\mathrm{m}}\varepsilon_{kl}^{\mathrm{m}}\,dV + \frac{1}{\mathrm{V_{RVE_4}}}\int_{\mathrm{V_{RVE_4}}} \mu_{in}^{\mathrm{m}}H_n^{\mathrm{m}}\,dV \end{aligned} \tag{2}$$

Here, it is assumed that an MRE has different RVEs depending on the considered phenomenon. Thus, $\mathrm{V_{RVE_1}}$ and $\mathrm{V_{RVE_4}}$ represent the volumes of the RVEs for a purely mechanical and purely magnetic phenomenon, while $\mathrm{V_{RVE_2}}$ and $\mathrm{V_{RVE_3}}$ are the RVEs for coupling phenomenon. The superscripts m and M denote the micro and macro level, respectively.

### 2.1. Microscopic Characterisation of MRE

As discussed above, the MRE is modelled as a heterogeneous material on the micro-scale. The constitutive equations of the components can be written in the same form as Eqs. (1) above:

$$\begin{aligned} \sigma_{ij}^{\mathrm{m}} &= C_{ijkl}^{\mathrm{m}}\varepsilon_{kl}^{\mathrm{m}} - Q_{nij}^{\mathrm{m}}H_n^{\mathrm{m}} \\ B_i^{\mathrm{m}} &= Q_{ikl}^{\mathrm{m}}\varepsilon_{kl}^{\mathrm{m}} + \mu_{in}^{\mathrm{m}}H_n^{\mathrm{m}} \end{aligned} \tag{3}$$

In this study, 2D MREs will be investigated on the micro-level, indicated with superscript m, to determine the RVE size. It is assumed that the RVE is polarized along the $z$-direction, and all internal forces act on the $xz$-plane. Adopting a plane stress assumption as well as matrix-vector notation, the stiffness, piezomagnetic coupling and permeability matrices of the transversely isotropic material read

$$\mathbf{C}^{\mathrm{m}} = \begin{bmatrix} C_{11} & C_{13} & 0 \\ C_{13} & C_{33} & 0 \\ 0 & 0 & C_{55} \end{bmatrix}, \quad \mathbf{Q}^{\mathrm{m}} = \begin{bmatrix} 0 & q_{31} \\ 0 & q_{33} \\ q_{15} & 0 \end{bmatrix}, \quad \boldsymbol{\mu}^{\mathrm{m}} = \begin{bmatrix} \mu_{11} & 0 \\ 0 & \mu_{33} \end{bmatrix} \tag{4}$$

Similarly, the kinematic relations, balance equations and governing equations can be written as

$$\boldsymbol{\varepsilon}^{\mathrm{m}} = \mathbf{L}_{\mathrm{u}}\mathbf{u}^{\mathrm{m}} \text{ and } \mathbf{H}^{\mathrm{m}} = -\mathbf{L}_{\varphi}\varphi^{\mathrm{m}} \tag{5}$$

$$\mathbf{L}_{\mathrm{u}}^{\mathrm{T}}\sigma^{\mathrm{m}} = \mathbf{0} \text{ and } \mathbf{L}_{\varphi}^{\mathrm{T}}\mathbf{B}^{\mathrm{m}} = \mathbf{0} \tag{6}$$

$$\begin{aligned} \mathbf{L}_{\mathrm{u}}^{\mathrm{T}}\mathbf{C}^{\mathrm{m}}\mathbf{L}_{\mathrm{u}}\mathbf{u}^{\mathrm{m}} + \mathbf{L}_{\mathrm{u}}^{\mathrm{T}}\mathbf{Q}^{\mathrm{m}}\mathbf{L}_{\varphi}\varphi^{\mathrm{m}} &= \mathbf{0} \\ \mathbf{L}_{\varphi}^{\mathrm{T}}\mathbf{Q}^{\mathrm{m}\mathrm{T}}\mathbf{L}_{\mathrm{u}}\mathbf{u}^{\mathrm{m}} - \mathbf{L}_{\varphi}^{\mathrm{T}}\mu^{\mathrm{m}}\mathbf{L}_{\varphi}\varphi^{\mathrm{m}} &= \mathbf{0} \end{aligned} \tag{7}$$

where $\mathbf{L}_{\varphi} = \nabla$ and $\mathbf{L}_{\mathrm{u}}$ is the usual strain-displacement derivative operator.

### 2.2. Finite Element Equations

To obtain the finite element formulation, the weak form of Eq. (7) can be written for domain $\Omega$ and boundary $\Gamma$ after integration by parts as follows:

$$\begin{aligned} \int_{\mathbf{\Omega}} (\mathbf{L}_{\mathrm{u}}\mathbf{w}_{\mathrm{u}})^{\mathrm{T}}\mathbf{C}^{\mathrm{m}}\mathbf{L}_{\mathrm{u}}\mathbf{u}^{\mathrm{m}}\mathrm{d}\Omega + \int_{\mathbf{\Omega}} (\mathbf{L}_{\mathrm{u}}\mathbf{w}_{\mathrm{u}})^{\mathrm{T}}\mathbf{Q}^{\mathrm{m}}\mathbf{L}_{\varphi}\varphi^{\mathrm{m}}\mathrm{d}\Omega &= \int_{\mathbf{\Gamma}} \mathbf{w}_{\mathrm{u}}^{\mathrm{T}}\mathbf{t}\mathrm{d}\Gamma \\ \int_{\mathbf{\Omega}} (\mathbf{L}_{\varphi}\mathrm{w}_{\varphi})^{\mathrm{T}}\mathbf{Q}^{\mathrm{m}\mathrm{T}}\mathbf{L}_{\mathrm{u}}\mathbf{u}^{\mathrm{m}}\mathrm{d}\Omega - \int_{\mathbf{\Omega}} (\mathbf{L}_{\varphi}\mathrm{w}_{\varphi})^{\mathrm{T}}\mu^{\mathrm{m}}\mathbf{L}_{\varphi}\varphi^{\mathrm{m}}\mathrm{d}\Omega &= \int_{\mathbf{\Gamma}} \mathrm{w}_{\varphi}^{\mathrm{T}}\mathbf{B}_{\perp}\mathrm{d}\Gamma \end{aligned} \tag{8}$$

where $\mathbf{w}_{\mathrm{u}}$ and $\mathrm{w}_{\varphi}$ are the test functions, $\mathbf{t}$ are the boundary tractions, and $\mathbf{B}_{\perp}$ is the magnetic traction on the boundary. Thus, the following system of equations is obtained:

$$\begin{bmatrix} \mathrm{K}_{\mathrm{uu}} & \mathrm{K}_{\mathrm{u}\varphi} \\ \mathrm{K}_{\varphi\mathrm{u}} & -\mathrm{K}_{\varphi\varphi} \end{bmatrix} \begin{bmatrix} \mathbf{d}^{\mathrm{m}} \\ \mathbf{\Psi}^{\mathrm{m}} \end{bmatrix} = \begin{bmatrix} \mathrm{F} \\ \Phi \end{bmatrix} \tag{9}$$

where $\mathbf{d}^{\mathrm{m}}$ and $\mathbf{\Psi}^{\mathrm{m}}$ are micro-scale nodal displacement and nodal scalar magnetic potential vectors via $\mathbf{u}^{\mathrm{m}} = \mathbf{N}_{\mathrm{u}}\mathbf{d}^{\mathrm{m}}$ and $\varphi^{m} = \mathbf{N}_{\varphi}\mathbf{\Psi}^{\mathrm{m}}$. Moreover, F and $\Phi$ are nodal mechanical force and nodal magnetic flux vectors. Lastly, stiffness matrices are given by

$$\begin{aligned} \mathbf{K}_{\mathrm{uu}} &= \int_{\mathbf{\Omega}} \mathbf{B}_{\mathrm{u}}^{\mathrm{T}}\mathbf{C}^{\mathrm{m}}\mathbf{B}_{\mathrm{u}}\mathrm{d}\mathbf{\Omega} \qquad \mathbf{K}_{\mathrm{u}\varphi} = \int_{\mathbf{\Omega}} \mathbf{B}_{\mathrm{u}}^{\mathrm{T}}\mathbf{Q}^{\mathrm{m}}\mathbf{B}_{\varphi}\mathrm{d}\mathbf{\Omega} \\ \mathbf{K}_{\varphi\mathrm{u}} &= \int_{\mathbf{\Omega}} \mathbf{B}_{\varphi}^{\mathrm{T}}\mathbf{Q}^{\mathrm{m}\mathrm{T}}\mathbf{B}_{\mathrm{u}}\mathrm{d}\mathbf{\Omega} \qquad \mathbf{K}_{\varphi\varphi} = \int_{\mathbf{\Omega}} \mathbf{B}_{\varphi}^{\mathrm{T}}\mu^{\mathrm{m}}\mathbf{B}_{\varphi}\mathrm{d}\mathbf{\Omega} \end{aligned} \tag{10}$$

with $\mathbf{B}_{\mathrm{u}} = \mathbf{L}_{\mathrm{u}}\mathbf{N}_{\mathrm{u}}$, $\mathbf{B}_{\varphi} = \mathbf{L}_{\varphi}\mathbf{N}_{\varphi}$. The matrices $\mathbf{N}_{\mathrm{u}}$ and $\mathbf{N}_{\varphi}$ contains the relevant shape functions.

After obtaining the nodal degrees of freedom, stress and magnetic induction in Eq. (3) can be calculated by following standard FE post-processing methods to be used for statistical analysis in the next section.

### 2.3. *Determination of RVE Size*

As it has been argued earlier in section 2, it is essential to determine the size of the RVE since it becomes a model parameter in the constitutive equations on the macro scale. This connection of RVE size and macroscopic constitutive equations will be explored and discussed in detail in section 4. In this section, the aim is to determine the RVE size by following the statistical method proposed by Gitman et al.[14]. As described in section 2.1, Eqs. (3-7) have been used to solve the RVE boundary value problem. The steps shown below are followed in this procedure to determine a lower bound of the RVE size.

The methodology consists of:

1. Creation of different realisations for the tested unit cell size with fixed inclusion diameter (Normal distribution of 100–300 µm in diameter is assumed) and volume fraction ($V_f$ = 30%) as seen in Figure 1. In our study, for an accurate statistical analysis, we created 200 realisations.

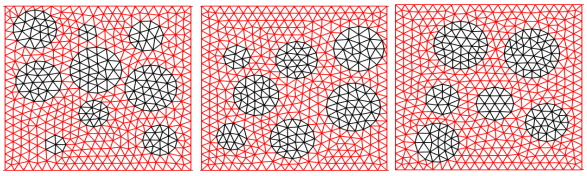

Figure 1: Different realisations of the unit cell (size 1x1 $mm^2$ and $V_f$ = 30%)

2. Application of loading conditions such as a tension test or magnetic loading as shown in Figure 2. The load is applied via prescribed nodal values of displacement U on the two corners on the left and right of the sample and/or magnetic potentials $\varphi$ on the left and right edges. Here, periodicity in boundary conditions has been implemented via penalty functions as given in [25].

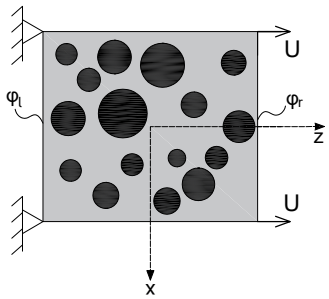


Figure 2: An RVE under external loadings

3. Performing the FE analysis and obtaining the parameter of interest, that is the averaged stress or the averaged magnetic induction along the $z$ direction over the RVE. At this point, the $z$ components of averaged stress and magnetic induction are evaluated since the maximum magnetostriction response is expected in this direction. Here, the different RVE sizes $L_1, L_2, L_3$ and $L_4$ are assessed separately as discussed in the introduction to section 2. In particular, $L_1$, which is the RVE size for purely mechanical terms in Eq. (22), is determined by applying the tension test and calculating the averaged stress in $z$ direction due to this loading. Similarly, the RVE size for a purely magnetic response, $L_4$, is assessed by calculating the averaged magnetic induction in $z$ direction due to the external magnetic loading. Lastly, the RVE sizes for coupling terms $L_2$ and $L_3$ are evaluated by obtaining the averaged stress results from external magnetic loading, and obtaining the averaged magnetic induction results from tension test respectively.
4. Finding the coefficient of variation value for the FE results.
5. Comparison of statistical analysis accuracy with the desired accuracy (which was taken 97% here).
6. Defining the tested size as the RVE size if the desired accuracy is obtained. Otherwise, increasing the unit cell size (Figure 3) and repeating the process.

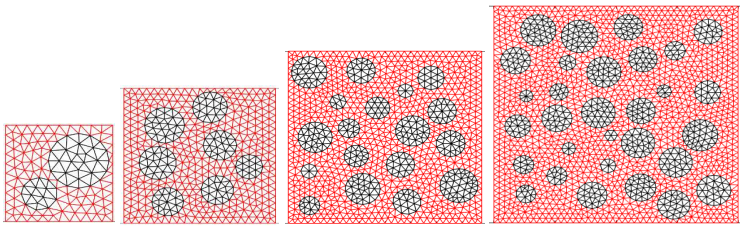

Figure 3: Different sizes of unit cells (from left to right: 0.5x0.5 mm$^2$, 1x1 mm$^2$, 1.5x1.5 mm$^2$, 2x2 mm$^2$ and $V_f$ = 30%)

## 3. Numerical Results and Discussion

The numerical experiments were conducted with a MATLAB code developed in-house. The material properties have been adopted from [26, 27] and are given in Table 1. In the calculation of the material constants for the magnetic particles, the procedure given by [24] was followed. Here, the matrix (polymer) is assumed as a non-magnetisable material. Because of this assumption, piezomagnetic constants were taken as zero to represent this behaviour. Also, the magnetic permeability of the matrix has been assumed to equal the magnetic permeability of the free space ($\mu_0 = 4\pi 10^{-6}$N/A$^2$) due to the same assumption.

| | $C_{11}$ | $C_{13}$ | $C_{33}$ | $C_{55}$ | $q_{31}$ | $q_{33}$ | $q_{15}$ | $\mu_{11}$ | $\mu_{33}$ |
|---|---|---|---|---|---|---|---|---|---|
| **Terfenol-D [26]** | 35 | 23 | 46 | 4 | -32.5 | 195 | 68.75 | 8.9 | 1.8 |
| **Polymer [27]** | 7.8 | 4.7 | 7.8 | 1.6 | 0 | 0 | 0 | $\mu_0$ | $\mu_0$ |

$C_{ij}$ in GPa, $q_{ij}$ in N/Am, $\mu_{ij}$ in $10^{-6}$N/A$^2$

Table 1: Material properties

Two hundred different realisations of each RVE size (from 0.5 to 2.5 mm) have been considered, and the responses of the RVEs have been obtained via finite element analysis by using three-node triangular elements. Following numerical analysis of all realisations, coefficients of variation have been calculated for each sample size to investigate the convergence of the results. This is a statistical measure of relative variability, and it is a useful statistic for comparing the degree of variation between data series. A lower value of the coefficient of variation means a more precise estimation. By comparing the coefficients of variation of computed parameters ($\sigma_{zz}$ or $B_z$) with the desired value, i.e. is 0.03 for 97% accuracy, a lower bound of the RVE can be defined as seen in Figure 4. As seen in the figure, once the desired accuracy and the results from the numerical tests have been plotted on the same graph, the intersection of the obtained values and chosen variability can be evaluated to define the RVE size.

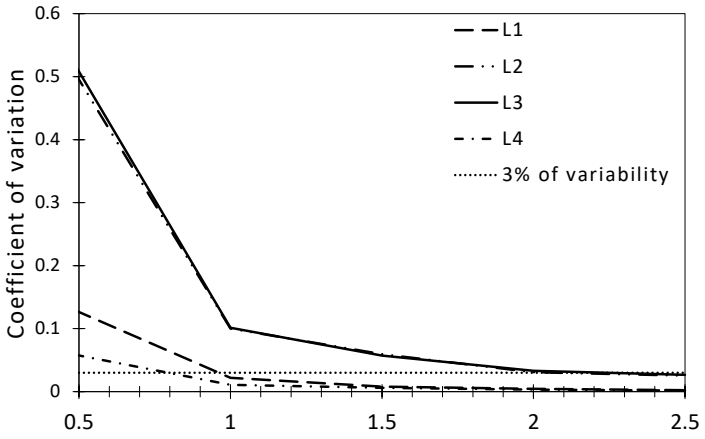


Figure 4: Convergence of the results

Realisations of each cell size (e.g. Figure 2) were subjected to mechanical and magnetic loading separately, and the steps given in section 2.3 were followed. Figure 4 shows converging trends around different values for predefined RVE sizes $L_1$, $L_2$, $L_3$ and $L_4$. It can be seen that the lower bound of the RVE can be considered as 1 mm for $L_1$, 0.9 mm for $L_4$, and 2.3 mm for $L_2$ and $L_3$. Furthermore, it is remarkable how small the difference between $L_2$ and $L_3$ is. This confirms the thermodynamic consistency requirements discussed later in section 4.

As shown above, it is possible to define an RVE size for an MRE material, and it is worthwhile to conduct a parametric study to investigate the effect of parameters on the RVE sizes such as contrast in stiffness, coupling and permeability properties of the constituents. It has already been shown for purely elastic material that the lower bound of the RVE size is affected by the stiffness ratio of the constituents [14]. Notably, changing the stiffness ratio, which also means increased heterogeneity, causes an increase in the lower bound of RVE. For this reason, a formalistic approach was established, and theoretical test specimens were created.

### *3.1. Contrast in Elastic Properties*

We now define the stiffness ratio $\beta_c$, as a ratio between inclusions and matrix stiffnesses, see Eq. (11). $\beta_c$ ranges (5, 25, 100) introduce a change in heterogeneity. This setup ensures that there will be factors of 5, 25 and 100 between the components' stiffness properties.

$$\beta_c = \frac{C_{inclusion}}{C_{matrix}} \tag{11}$$

Figure 5 shows the effect of the elastic stiffness ratios on the RVE sizes. It can be seen that there is a positive correlation between the contrast and the lower bound of the RVE size up to a certain value of $L_1$ that represents the purely mechanical RVE size. When the contrast ratio is increased from 5 to 25, the lower bound of RVE size has values of around 1 and 1.4 mm, respectively. However, increasing the stiffness contrast to more than 25 does not lead a notable further change. Furthermore, it was found that different contrast values in stiffness result in near identical RVE sizes for the coupling and purely magnetic RVE sizes $L_2$, $L_3$ and $L_4$, which means that the stiffness contrast does not affect those RVE sizes.

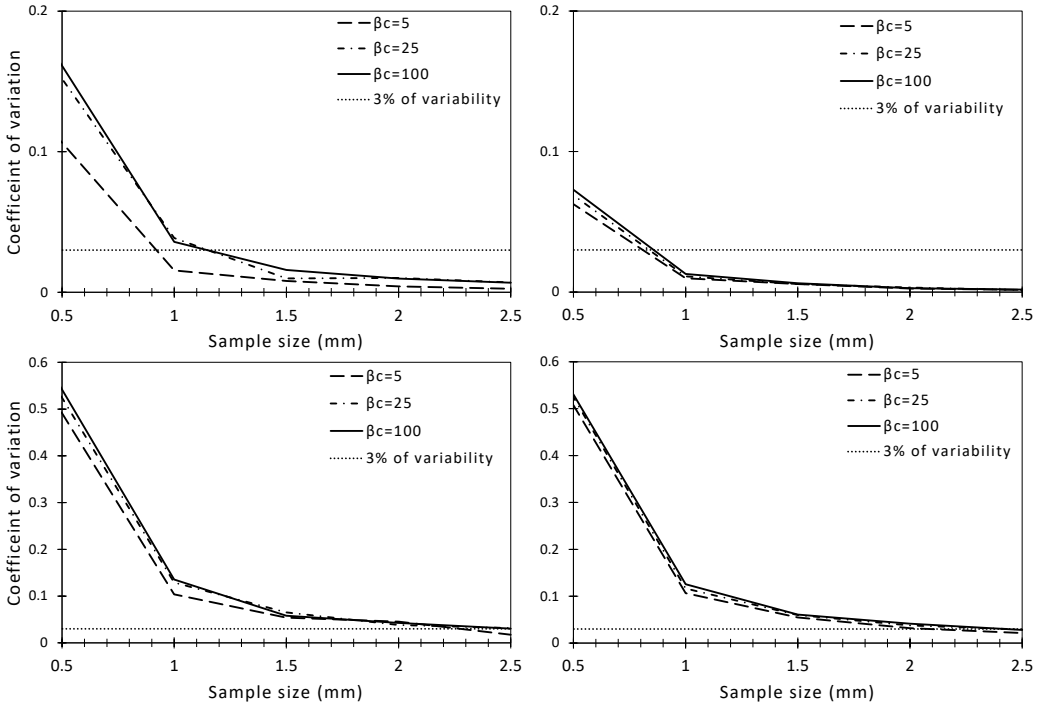


Figure 5: RVE sizes for different stiffness contrast values. $L_1$ (top left), $L_2$ (bottom left), $L_3$ (bottom right) and $L_4$ (top right).

### 3.2. Contrast in Magnetic Properties

Similarly, the contrast in piezomagnetic and magnetic permeability can be obtained via the ratios $\beta_{\mathrm{q}}$ and $\beta_{\mu}$.

$$\beta_{\mathrm{q}} = \frac{\mathrm{Q}_{\mathrm{inclusion}}}{\mathrm{Q}_{\mathrm{matrix}}} \quad , \quad \beta_{\mu} = \frac{\mu_{\mathrm{inclusion}}}{\mu_{\mathrm{matrix}}} \tag{12}$$

Figure 6 shows the influence of the piezomagnetic coupling contrast. Here, the stiffness contrast was chosen as 5 and the magnetic permeability contrasts were kept constant ($\beta_{\mu_{11}} = 8.9, \beta_{\mu_{33}} = 1.8$, see Table 1). It has been observed that more contrast in coupling properties of the constituents leads to larger RVE sizes $L_2$ and $L_3$ only, with minimal effects on $L_1$ and $L_4$.

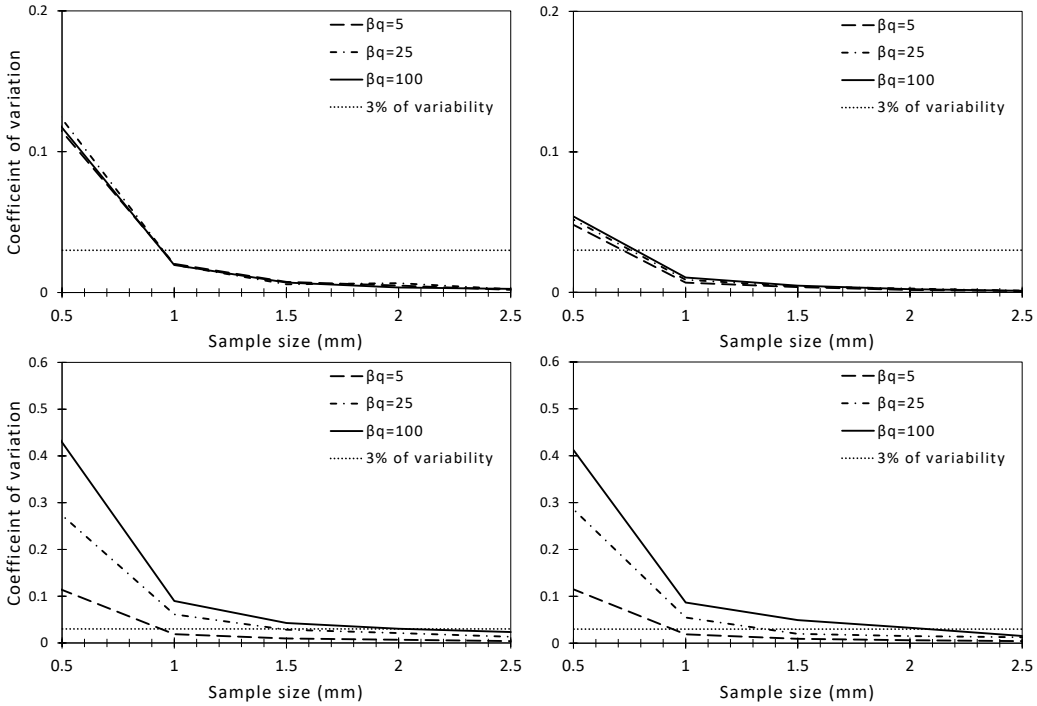


Figure 6: RVE sizes for different piezomagnetic contrast values. $L_1$ (top left), $L_2$ (bottom left), $L_3$ (bottom right) and $L_4$ (top right).

The contrast in magnetic permeability is the basis of the next test setup and Figure 7 presents the result of this configuration. Analogous to the previous case, piezomagnetic coupling contrast was kept constant at the values given in Table 1, and the stiffness contrast was assumed as 5 to study only the effect of the permeability. Similarly, the results show that contrast in magnetic permeability has an effect on the RVE size $L_4$, and this trend is similar to stiffness contrast for $L_1$.

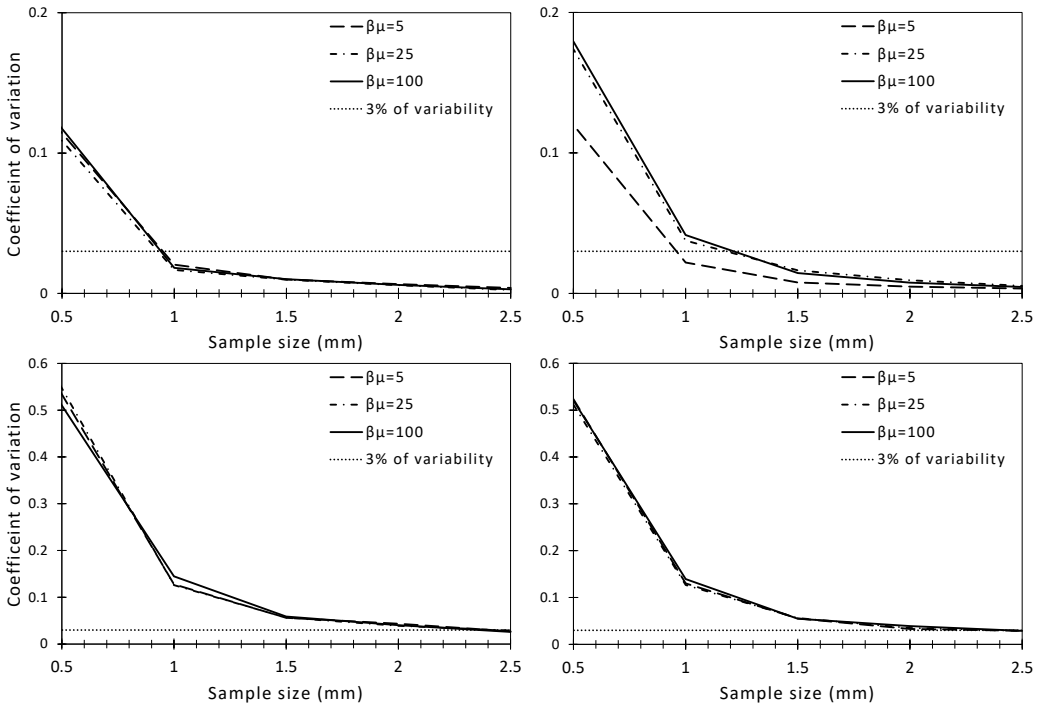


Figure 7: RVE sizes for different permeability contrast values. $L_1$ (top left), $L_2$ (bottom left), $L_3$ (bottom right) and $L_4$ (top right).

In addition to contrasts of 5, 25 and 100, it is relevant to investigate larger contrast values to understand the influence better. As seen in Figure 8, more contrasts have been introduced to stiffness, coupling and permeability. The pattern in the coupling contrast increase for $L_2$ and $L_3$ is different and it shows a continuously increasing RVE size. However, the difference between the RVE sizes for larger permeability and stiffness contrasts for $L_4$ and $L_1$ is relatively insignificant compared to other cases beyond a value of 100. Here, it can be concluded that RVE sizes are dependent on the stiffness, coupling and permeability contrast of the constituents which means heterogeneity in these properties is an effective parameter for the related RVE size.

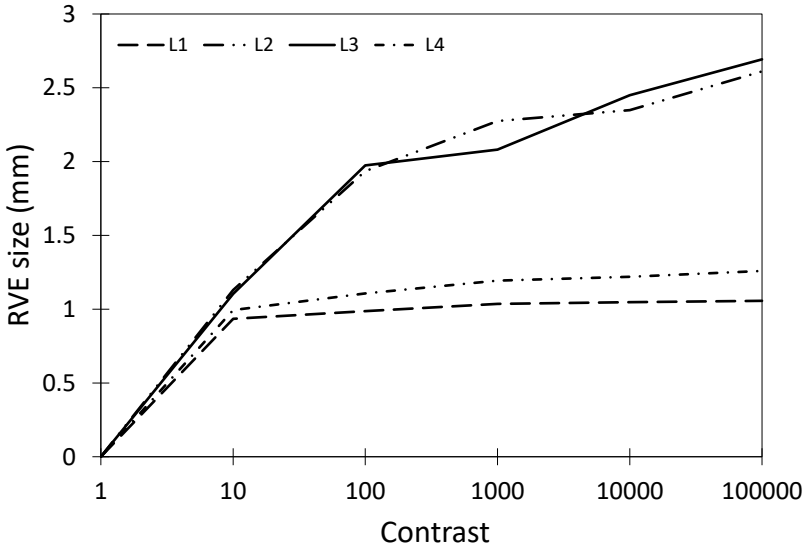


Figure 8: RVE sizes for larger contrast values

Overall, separately considered RVE sizes for an MRE material can be determined by following the statistical analysis as given in this section. Moreover, it has been shown that the contrast between the elastic and magnetic properties of the constituents is an effective parameter for the related RVE sizes. However, the pattern of this effectiveness is different for coupling and purely elastic/magnetic RVEs.

## 4. Homogenisation and Macroscopic Length Scale Parameter

In contrast to heterogeneous micro-level, MRE is considered as a homogeneous piezomagnetic material with effective material properties on the macro-level. Besides, the relation between the macroscopic stress/induction and microscopic counterparts has been defined in Eq. (2). After determining and analysing the properties of the RVE sizes as presented in previous section, it is now possible to derive the macroscopic constitutive and governing equations by using Eq. (2) and the secon-order homogenisation scheme. Consequently, the formulation of a fully coupled magneto-mechanical model with gradients in terms of RVE size can be obtained to introduce the micro structural information to the macro scale.

The associated local coordinate systems are assumed to have their origin at the centre of the RVE. Before applying second-order homogenisation, linearisations of spatially dependent stiffness, strain, coupling, permeability and magnetic field can be presented as

$$\begin{aligned} C^{\mathrm{m}}_{ijkl} &= C^{\mathrm{M}}_{ijkl} + C^{\mathrm{M}}_{ijkl,o}\delta x_o \\ \varepsilon^{\mathrm{m}}_{kl} &= \varepsilon^{\mathrm{M}}_{kl} + \varepsilon^{\mathrm{M}}_{kl,p}\delta x_p \\ Q^{\mathrm{m}}_{nij} &= Q^{\mathrm{M}}_{nij} + Q^{\mathrm{M}}_{nij,o}\delta x_o \\ H^{\mathrm{m}}_{n} &= H^{\mathrm{M}}_{n} + H^{\mathrm{M}}_{n,p}\delta x_p \\ \mu^{\mathrm{m}}_{in} &= \mu^{\mathrm{M}}_{in} + \mu^{\mathrm{M}}_{in,o}\delta x_o \end{aligned} \tag{13}$$

It is noted that first-order homogenisation can be obtained if only the first terms on the right hand-sides of Eq. (13) are considered. This yields $\mathrm{X}^{\mathrm{m}} = \mathrm{X}^{\mathrm{M}}$, where X is stiffness, strain, coupling, permeability or magnetic field. However, second-order homogenisation requires the introduction of second-order terms with $\delta x$. Now the constitutive relation for the macroscopic stress and magnetic induction (Eq. (2)) can be rewritten as

$$\begin{aligned} \sigma^{\mathrm{M}}_{ij} =& \frac{1}{\mathrm{V}_{\mathrm{RVE}_1}} \int_{\mathrm{V}_{\mathrm{RVE}_1}} (C^{\mathrm{M}}_{ijkl}\varepsilon^{\mathrm{M}}_{kl} + C^{\mathrm{M}}_{ijkl}\varepsilon^{\mathrm{M}}_{kl,p}\delta x_p + C^{\mathrm{M}}_{ijkl,o}\varepsilon^{\mathrm{M}}_{kl}\delta x_o + C^{\mathrm{M}}_{ijkl,o}\varepsilon^{\mathrm{M}}_{kl,p}\delta x_o\delta x_p) \\ & - \frac{1}{\mathrm{V}_{\mathrm{RVE}_2}} \int_{\mathrm{V}_{\mathrm{RVE}_2}} (Q^{\mathrm{M}}_{nij}H^{\mathrm{M}}_{n} + Q^{\mathrm{M}}_{nij}H^{\mathrm{M}}_{n,p}\delta x_p + Q^{\mathrm{M}}_{nij,o}H^{\mathrm{M}}_{n}\delta x_o + Q^{\mathrm{M}}_{nij,o}H^{\mathrm{M}}_{n,p}\delta x_o\delta x_p) \\ B^{\mathrm{M}}_{i} =& \frac{1}{\mathrm{V}_{\mathrm{RVE}_3}} \int_{\mathrm{V}_{\mathrm{RVE}_3}} (Q^{\mathrm{M}}_{ikl}\varepsilon^{\mathrm{M}}_{kl} + Q^{\mathrm{M}}_{ikl}\varepsilon^{\mathrm{M}}_{kl,p}\delta x_p + Q^{\mathrm{M}}_{ikl,o}\varepsilon^{\mathrm{M}}_{kl}\delta x_o + Q^{\mathrm{M}}_{ikl,o}\varepsilon^{\mathrm{M}}_{kl,p}\delta x_o\delta x_p) \\ & + \frac{1}{\mathrm{V}_{\mathrm{RVE}_4}} \int_{\mathrm{V}_{\mathrm{RVE}_4}} (\mu^{\mathrm{M}}_{in}H^{\mathrm{M}}_{n} + \mu^{\mathrm{M}}_{in}H^{\mathrm{M}}_{n,p}\delta x_p + \mu^{\mathrm{M}}_{in,o}H^{\mathrm{M}}_{n}\delta x_o + \mu^{\mathrm{M}}_{in,o}H^{\mathrm{M}}_{n,p}\delta x_o\delta x_p) \end{aligned} \tag{14}$$

In Eq. (14), $C^{\mathrm{M}}_{ijkl}$, $\varepsilon^{\mathrm{M}}_{kl}$, $Q^{\mathrm{M}}_{nij}$, $Q^{\mathrm{M}}_{ikl}$,$\mu^{\mathrm{M}}_{in}$ and $H^{\mathrm{M}}_{n}$ can be taken out of the integral since they are the values at the centre of the RVEs. Assuming a square RVE with its centre acting as origin of a Cartesian coordinate system, the linear terms of $\delta x$ cancel as they consist of odd functions integrated over a symmetric domain. The quadratic terms are integrated by parts as follows

$$
\begin{aligned}
\int_{V_{RVE_1}} C^M_{ijkl,o}\varepsilon^M_{kl,p}\delta x_o\delta x_p &= \int_S C^M_{ijkl}\varepsilon^M_{kl,p}n_o\delta x_o\delta x_p dS \;-\; \int_{V_{RVE_1}} (C^M_{ijkl}\varepsilon^M_{kl,op}\delta x_o\delta x_p \\
&\quad + C^M_{ijkl}\varepsilon^M_{kl,p}\delta x_{o,o}\delta x_p + C^M_{ijkl}\varepsilon^M_{kl,p}\delta x_o\delta x_{p,o})dV \\
\int_{V_{RVE_2}} Q^M_{nij,o}H^M_{n,p}\delta x_o\delta x_p &= \int_S Q^M_{nij}H^M_{n,p}n_o\delta x_o\delta x_p dS \;-\; \int_{V_{RVE_2}} (Q^M_{nij}H^M_{n,op}\delta x_o\delta x_p \\
&\quad + Q^M_{nij}H^M_{n,p}\delta x_{o,o}\delta x_p + Q^M_{nij}H^M_{n,p}\delta x_o\delta x_{p,o})dV \\
\int_{V_{RVE_3}} Q^M_{ikl,o}\varepsilon^M_{kl,p}\delta x_o\delta x_p &= \int_S Q^M_{ikl}\varepsilon^M_{kl,p}n_o\delta x_o\delta x_p dS \;-\; \int_{V_{RVE_3}} (Q^M_{ikl}\varepsilon^M_{kl,op}\delta x_o\delta x_p \\
&\quad + Q^M_{ikl}\varepsilon^M_{kl,p}\delta x_{o,o}\delta x_p + Q^M_{ikl}\varepsilon^M_{kl,p}\delta x_o\delta x_{p,o})dV \\
\int_{V_{RVE_4}} \mu^M_{in,o}H^M_{n,p}\delta x_o\delta x_p &= \int_S \mu^M_{in}H^M_{n,p}n_o\delta x_o\delta x_p dS \;-\; \int_{V_{RVE_4}} (\mu^M_{in}H^M_{n,op}\delta x_o\delta x_p \\
&\quad + \mu^M_{in}H^M_{n,p}\delta x_{o,o}\delta x_p + \mu^M_{in}H^M_{n,p}\delta x_o\delta x_{p,o})dV
\end{aligned}
\tag{15}
$$

Assuming periodic boundary conditions, the boundary integrals vanish and the last two terms in each of Eq. (15) vanish since they consist of odd functions. Furthermore, the integrals with $\delta x_o\delta x_p$ can be evaluated as

$$
\int_{V_{RVE_i}} \delta x_o\delta x_p dV = \int_{-\frac{L_i}{2}}^{\frac{L_i}{2}}\int_{-\frac{L_i}{2}}^{\frac{L_i}{2}}\int_{-\frac{L_i}{2}}^{\frac{L_i}{2}} \delta x_o\delta x_p dx_1dx_2dx_3 = \frac{1}{12}L_i^5\delta_{op} \qquad (i=1,2,3,4) \tag{16}
$$

where $\delta_{op}$ is the kronecker delta, $V_{RVE_i} = L_i^3$ and $L_i$ is the size of the $i$th RVE.

With these elaborations, the piezomagnetic macroscopic constitutive equations with gradients of strain, magnetic field, and magneto-mechanical coupling terms can be expressed as

$$
\begin{aligned}
\sigma^M_{ij} &= C^M_{ijkl}\left(\varepsilon^M_{kl} - \frac{L_1^2}{12}\varepsilon^M_{kl,pp}\right) - Q^M_{nij}\left(H^M_n - \frac{L_2^2}{12}H^M_{n,pp}\right) \\
B^M_i &= Q^M_{ikl}\left(\varepsilon^M_{kl} - \frac{L_3^2}{12}\varepsilon^M_{kl,pp}\right) + \mu^M_{in}\left(H^M_n - \frac{L_4^2}{12}H^M_{n,pp}\right)
\end{aligned}
\tag{17}
$$

In addition to the material coefficients of macroscopic constitutive equations Eq. (17), there are length scale parameters (in terms of $RVE_i$ size $L_i$). It must be pointed out that Eqs. (2,13-17) have been derived to motivate and present the application of the determined RVE sizes in the previous section. As the aim of this study, the parameters $L_i$ (i=1,2,3,4) were determined by a statistical analysis of a boundary value problem on the micro-level as shown in section 3.

Note that Eq. (17) follows the structure of the gradient enriched piezomagnetic model proposed by Xu et. al [8], e.g.

$$
\begin{aligned}
\sigma_{ij} &= C_{ijkl}(\varepsilon_{kl} - \ell_1^2\varepsilon_{kl,mm}) - q_{ijk}(H_k - \ell_2^2 H_{k,mm}) \\
B_i &= q_{ijk}(\varepsilon_{jk} - \ell_3^2\varepsilon_{jk,mm}) + \mu_{ij}(H_j - \ell_4^2 H_{j,mm})
\end{aligned}
\tag{18}
$$

Comparing eq. (17) and eq. (18), it can be seen that the link between phenomenological parameters, representing internal length scales $\ell_i$ and RVE sizes $L_i$ can be established.

$$\ell_i^2 = \frac{L_i^2}{12} \tag{19}$$

The authors of [8] followed a variational formulation, which led to $L_2 = L_3$ for reasons of thermodynamic consistency. Here, this issue has been explored in section 3 by determining the same size for the coupling RVEs $L_2$ and $L_3$. As following section 3, it can be seen that $L_2$ and $L_3$ typically are larger than $L_1$ and $L_4$, for practical purposes, it may be assumed that $L_1 = L_2 = L_3 = L_4 = L$, which satisfies all test setups according to numerical results.

Eventually, the field equations of the problem on the macro scale can be obtained by combining the usual kinematic relations, balance equations and constitutive equations:

$$\varepsilon_{ij}^{\mathrm{M}} = \frac{1}{2}(u_{i,j}^{\mathrm{M4}pt} + u_{j,i}^{\mathrm{M4}pt}) \text{ and } H_i^{\mathrm{M4}pt} = -\varphi_{,i}^{\mathrm{M4}pt} \tag{20}$$

$$\sigma_{ij,j}^{\mathrm{M}} = 0 \text{ and } B_{i,i}^{\mathrm{M}} = 0 \tag{21}$$

where $u_i^{\mathrm{M4}pt}$ is the displacement field and $\varphi^{\mathrm{M4}pt}$ is the scalar magnetic potential on the macro-level; and the governing equations are

$$\begin{aligned} C_{ijkl}^{\mathrm{M}}\left(u_{k,jl}^{\mathrm{M4}pt} - \frac{L^2}{12}u_{k,jlpp}^{\mathrm{M4}pt}\right) + Q_{nij}^{\mathrm{M}}\left(\varphi_{,jn}^{\mathrm{M4}pt} - \frac{L^2}{12}\varphi_{,jnpp}^{\mathrm{M4}pt}\right) = 0 \\ Q_{ikl}^{\mathrm{M}}\left(u_{k,il}^{\mathrm{M4}pt} - \frac{L^2}{12}u_{k,ilpp}^{\mathrm{M4}pt}\right) - \mu_{in}^{\mathrm{M}}\left(\varphi_{,in}^{\mathrm{M4}pt} - \frac{L^2}{12}\varphi_{,inpp}^{\mathrm{M4}pt}\right) = 0 \end{aligned} \tag{22}$$

with $L$ chosen the largest of the four RVEs sizes.

## 5. Conclusions

In this study, a piezomagnetic continuum model has been developed with gradients of strain, piezo-magnetic coupling and magnetic field whereby the microstructural length scale parameters are expressed in terms of RVE sizes. To determine the RVE size, the method proposed by Gitman et al. [14] has been followed for an MRE model on the micro level, and the influence of the some parameters such as contrast in stiffness, coupling and permeability properties of the constituents have been studied.

The proposed statistical analysis can be used to determine lower bounds of the RVE size for an MRE material. Here, four different RVE sizes were postulated for different phenomena namely $L_1$ for purely elastic, $L_4$ for purely magnetic, and $L_2$ and $L_3$ for coupling behaviour in the material. In line with thermodynamic consistency, the difference between the lower bound of $L_2$ and $L_3$ was found to be negligible, however the determined RVE sizes for $L_1$ and $L_4$ are clearly smaller and different. It may be suggested that using the largest determined RVE sizes for $L_2$ or $L_3$ also covers the lower bound condition of the other RVE sizes and only this size can be used in gradient enriched governing equations (Eq. 22) to introduce the information from the micro level.

The formalistic approach showed that the contrast in material properties of the constituents can affect the minimum RVE sizes. It was found that the increase in stiffness contrast leads to larger values of $L_1$, whereas there is no influence on the others. Similarly, the same trend was observed for an increase in coupling and permeability contrasts for the RVE sizes $L_2$ or $L_3$, and $L_4$ respectively. It can be concluded that for more heterogeneity in these material properties, larger sizes of the associated RVE are obtained.

Finally, there is a converging trend for $L_1$ and $L_4$, but $L_2$ and $L_3$ show a non-convergent trend in the range of assumed larger contrast values. Given that the difference between convergent $L_1$ and $L_4$ and non-convergent $L_2$ and $L_3$ occurs for extremely large contrast, for practical purposes one may assume $L_1 = L_2 = L_3 = L_4$.

## Acknowledgements

This research did not receive any specific grant from funding agencies in the public, commercial, or not-for-profit sectors.

## 6. Data availability

The raw/processed data required to reproduce these findings cannot be shared at this time as the data also forms part of an ongoing study.

## References


[1] J. Thévenot, H. Oliveira, O. Sandre, S. Lecommandoux, Chemical Society Reviews 42 (2013) 7099–7116. URL: http://dx.doi.org/10.1039/C3CS60058K. doi:10.1039/C3CS60058K.

[2] G. Filipcsei, I. Csetneki, A. Szilágyi, M. Zrínyi, Magnetic Field-Responsive Smart Polymer Composites, Springer Berlin Heidelberg, 2007, pp. 137–189. URL: https://doi.org/10.1007/12_2006_104. doi:10.1007/12_2006_104.

[3] L. Taixiang, X. Yangguang, in: Smart and Functional Soft Materials, IntechOpen, 2019. URL: https://doi.org/10.5772/intechopen.85083. doi:10.5772/intechopen.85083.

[4] R. Elhajjar, C. Law, A. Pegoretti, Progress in Materials Science 97 (2018) 204 – 229. URL: http://www.sciencedirect.com/science/article/pii/S0079642518300185. doi:https://doi.org/10.1016/j.pmatsci.2018.02.005.

[5] N. Ekreem, A. Olabi, T. Prescott, A. Rafferty, M. Hashmi, Journal of Materials Processing Technology 191 (2007) 96 – 101. URL: http://www.sciencedirect.com/science/article/pii/S0924013607002889. doi:https://doi.org/10.1016/j.jmatprotec.2007.03.064.

[6] T. Liu, T. Chan, K. Wang, H. Tsou, RSC Advances 5 (2015) 90098–90102. URL: http://dx.doi.org/10.1039/C5RA17306J. doi:10.1039/C5RA17306J.

[7] L. C. Davis, Journal of Applied Physics 85 (1999) 3348–3351. URL: https://doi.org/10.1063/1.369682. doi:10.1063/1.369682.

[8] M. Xu, I. M. Gitman, H. Askes, Computers and Structures 212 (2019) 275–288. URL: https://doi.org/10.1016/j.compstruc.2018.11.004. doi:10.1016/j.compstruc.2018.11.004.

[9] D. S. Wood, P. J. Camp, Physical Review E 83 (2011) 011402. URL: https://link.aps.org/doi/10.1103/PhysRevE.83.011402. doi:10.1103/PhysRevE.83.011402.

[10] A. Bastola, V. Hoang, L. Li, Materials Design 114 (2017) 391 – 397. URL: http://www.sciencedirect.com/science/article/pii/S0264127516313922. doi:https://doi.org/10.1016/j.matdes.2016.11.006.

[11] A. Attaran, J. Brummund, T. Wallmersperger, Journal of Magnetism and Magnetic Materials 431 (2017) 188 – 191. URL: http://www.sciencedirect.com/science/article/pii/S0304885316321643. doi:https://doi.org/10.1016/j.jmmm.2016.09.058.

[12] K. A. Kalina, P. Metsch, M. Kästner, International Journal of Solids and Structures 102-103 (2016) 286 – 296. URL: http://www.sciencedirect.com/science/article/pii/S0020768316303109. doi:https://doi.org/10.1016/j.ijsolstr.2016.10.019.

[13] Y. L. Raikher, O. V. Stolbov, Journal of Physics: Condensed Matter 20 (2008) 204126. URL: https://doi.org/10.1088%2F0953-8984%2F20%2F20%2F204126. doi:10.1088/0953-8984/20/20/204126.

[14] I. M. Gitman, Representative volumes and multi-scale modelling of quasi-brittle materials, Doctoral thesis, Technische Universiteit Delft, 2006. URL: https://repository.tudelft.nl/islandora/object/uuid:b9073796-fd46-433f-a405-1b226ce9583a?collection=research.

[15] P. Metsch, K. A. Kalina, C. Spieler, M. Kästner, Computational Materials Science 124 (2016) 364 – 374. URL: http://www.sciencedirect.com/science/article/pii/S0927025616303822. doi:https://doi.org/10.1016/j.commatsci.2016.08.012.

[16] S. Sun, X. Peng, Z. Guo, Advances in Condensed Matter Physics (2014). URL: https://www.hindawi.com/journals/acmp/2014/232510/. doi:https://doi.org/10.1155/2014/232510.

[17] W. H. Li, X. Z. Zhang, Smart Materials and Structures 19 (2010) 035002. URL: https://doi.org/10.1088%2F0964-1726%2F19%2F3%2F035002. doi:10.1088/0964-1726/19/3/035002.

[18] D. Borin, S. Odenbach, G. Stepanov, Journal of Magnetism and Magnetic Materials 470 (2019) 85 – 88. URL: http://www.sciencedirect.com/science/article/pii/S030488531732752X. doi:https://doi.org/10.1016/j.jmmm.2017.12.072.

[19] I. Gitman, H. Askes, L. Sluys, in: Fifth international conference on fracture mechanics of concrete and concrete structures, La-FraMCos, 2004, pp. 483–491.

[20] L. Ke, Y. Wang, J. Yang, S. Kitipornchai, Acta Mechanica Sinica 30 (2014) 516–525. URL: https://doi.org/10.1007/s10409-014-0072-3. doi:10.1007/s10409-014-0072-3.

[21] I. M. Gitman, H. Askes, E. Aifantis, Journal of the Mechanical Behavior of Materials 18 (2007) 1–16. URL: https://www.degruyter.com/view/journals/jmbm/18/1/article-p1.xml.

[22] Y. Pang, J. Liu, Y. Wang, D. Fang, Acta Mechanica Solida Sinica 21 (2008) 483 – 490. URL: http://www.sciencedirect.com/science/article/pii/S0894916609602524. doi:https://doi.org/10.1007/s10338-008-0858-6.

[23] M. Lan, P. Wei, Acta Mechanica 225 (2014). URL: https://doi.org/10.1007/s00707-013-0984-1.

[24] H. Mane, Mathematical Modeling and Numerical Simulation of Magnetoelastic Coupling, Doctoral thesis, Technische Universität Kaiserslautern, 2019. URL: http://nbn-resolving.de/urn:nbn:de:hbz:386-kluedo-55199.

[25] H. Askes, S. Piercy, S. Ilanko, Communications in Numerical Methods in Engineering 24 (2008) 1163–1169. URL: https://onlinelibrary.wiley.com/doi/abs/10.1002/cnm.1023. doi:https://doi.org/10.1002/cnm.1023. arXiv:https://onlinelibrary.wiley.com/doi/pdf/10.1002/cnm.1023.

[26] F. Claeyssen, N. Lhermet, F. Barillot, R. Letty, ISAGMM 2006 CONF (2006). URL: https://www.cedrat-technologies.com/fileadmin/user_upload/CTEC/Publications/Publications/2006/10/ISAGMM2006_Magnetostrictive_Actuators_Transducers_Giant_Strains.pdf.

[27] Y. Z. Wang, F. M. Li, W. H. Huang, X. Jiang, Y. S. Wang, K. Kishimoto, International Journal of Solids and Structures 45 (2008) 4203 – 4210. URL: http://www.sciencedirect.com/science/article/pii/S0020768308001017. doi:https://doi.org/10.1016/j.ijsolstr.2008.03.001.